Paleoceanography and Paleoclimatology

RESEARCH ARTICLE
10.1029/2020PA004107

Key Points:

- Brazil Current heat transport coupled to changes in strength of the Atlantic Meridional Overturning Circulation during the last deglacial
- Antiphased heat transport by the Brazil and North Brazil Currents during Heinrich Event 1
- Warming of western tropical South Atlantic sea surface based on foraminiferal Mg/Ca exceeds numerical model results for Heinrich Event 1

Supporting Information:

Supporting Information may be found in the online version of this article.

Correspondence to:

K. J. F. Meier,
karl.meier@geow.uni-heidelberg.de

Citation:

Meier, K. J. F., Bahr, A., Chiessi, C. M., Albuquerque, A. L., Raddatz, J., & Friedrich, O. (2021). Role of the tropical Atlantic for the interhemispheric heat transport during the last deglaciation. *Paleoceanography and Paleoclimatology*, *36*, e2020PA004107. https://doi.org/10.1029/2020PA004107

Received 3 SEP 2020
Accepted 11 MAR 2021

Role of the Tropical Atlantic for the Interhemispheric Heat Transport During the Last Deglaciation

Karl J. F. Meier[1], André Bahr[1], Cristiano M. Chiessi[2], Ana Luiza Albuquerque[3], Jacek Raddatz[4], and Oliver Friedrich[1]

[1]Institute of Earth Sciences, Heidelberg University, Heidelberg, Germany, [2]School of Arts, Sciences and Humanities, University of São Paulo, São Paulo, Brazil, [3]Programa de Geociências (Geoquímica), Universidade Federal Fluminense, Niterói, Brazil, [4]Institute of Geosciences, Goethe University Frankfurt, Frankfurt, Germany

Abstract During the last deglaciation abrupt millennial-scale perturbations of the Atlantic Meridional Overturning Circulation massively altered the interhemispheric heat distribution affecting, for example, continental ice volume and hydroclimate. If and how the related cross-equatorial heat transport was controlled by the interplay between the southward-flowing Brazil Current (BC) and northward-flowing North Brazil Current (NBC) remains controversial. To assess the role of tropical heat transport during the last deglaciation, we obtained a high-resolution foraminiferal Mg/Ca-based sea surface temperature (SST) record from the BC domain at 21.5°S. The data reveal a yet undocumented warming of at least 4.6°C of the BC during Heinrich Stadial 1 at ~16 ka indicating massive oceanic heat accumulation in the tropical South Atlantic. Simultaneously, a strongly diminished NBC prevented the release of this excess heat into the northern tropics. The observed magnitude of heat accumulation substantially exceeds numerical model simulations, stressing the need to further scrutinize atmospheric and oceanic heat transport during extreme climatic events.

Plain Language Summary The Atlantic overturning circulation underwent abrupt millennial-scale perturbations. Such phases of sluggish oceanic circulation resulted in a substantial reduction of northward heat transport. As a consequence, substantial cooling occurred in the Northern Hemisphere and warming occurred in the Southern Hemisphere with severe effects on tropical precipitation. The distribution of heat within the western tropical Atlantic is accomplished by the southward-flowing BC and the northward-flowing NBC. By reconstructing SSTs for the interval between 20,000 and 10,000 yr before present, we assess the role of both currents in the interhemispheric heat transport during weak Atlantic overturning. We found that a sluggish overturning circulation resulted in anomalous southward heat transport by the BC in concert with a weak NBC, which lead to a yet undocumented warming of at least 4.6°C in the western tropical South Atlantic. This warming significantly exceeds reconstructions based on numerical simulations. This points to the need to further improve our understanding of changes in the cross-equatorial oceanic and atmospheric heat transport in response to rapid changes in ocean circulation, in particular as a significant weakening of the Atlantic overturning circulation is predicted in the wake of anthropogenic climate change.

1. Introduction

A pervasive feature of rapid millennial-scale climatic perturbations during glacial terminations is the thermal bipolar seesaw which describes the interhemispheric imbalance in global heat distribution (Broecker, 1998; Stocker, 1998). This thermal asymmetry arises from the substantial fresh-water forced weakening of the Atlantic Meridional Overturning Circulation (AMOC) which in turn diminishes the northward oceanic heat transport (OHT) (Crowley, 1992; McManus et al., 2004; Stocker & Johnsen, 2003). Sluggish northward OHT leads to cooling of the North Atlantic surface such as during Heinrich Stadials (HS). Within HS short phases (centennial to millennial time-scales) of massive discharges of icebergs to the North Atlantic and an almost complete shut-down of the AMOC typify Heinrich Events that represent the time of the most intense state of Northern Hemisphere cooling (Bond et al., 1992; Heinrich, 1988; McManus et al., 2004). One of the latest of such Northern Hemispheric cooling events was Heinrich Event 1a (HE1a) around 16 ka, indicated by a distinct layer of ice-rafted detritus (IRD) found at the Iberian Margin (Bard et al., 2000).

Simultaneously to the northern cooling, the surface waters of the South Atlantic warm up as evidenced from extratropical sea surface temperature (SST) records (Barker et al., 2009; Chiessi et al., 2015).

The surface current systems of the western tropical Atlantic play a crucial role for controlling the interhemispheric distribution of oceanic heat. The southward heat transport is accomplished by the Brazil Current (BC), while the northward-flowing North Brazil Current (NBC) constitutes a bottleneck of the upper AMOC return flow as it is responsible for the northward OHT (Peterson & Stramma, 1991; Rühs et al., 2015; Zhang et al., 2011). It has been suggested that both, BC and NBC, are anti-phased as the BC invigorates (weakens) while the NBC diminishes (strengthens) during sluggish (strong) AMOC, promoting heat accumulation in the South Atlantic (Arz et al., 1998, 1999). Numerous freshwater-hosing modeling experiments were used to examine the response of the coupled atmosphere-oceanic system during HS1-like events. These numerical models consensually showed that warming of the sea surface occurred in the tropical South Atlantic with a magnitude of up to 2°C, in line with an extreme southward shift of the Intertropical Convergence Zone (ITCZ) (e.g., Chang et al., 2008; Dahl et al., 2005; Deplazes et al., 2013; Zhang & Delworth, 2005). The southward shift of the ITCZ results from increased northward atmospheric heat transport (AHT) into the colder hemisphere during phases of weak AMOC that is necessary to compensate the interhemispheric heat imbalance, and is in line with an anomalous intensification and a cross-equatorial extension of the Northern Hemisphere Hadley-Cell (Donohoe et al., 2012; McGee et al., 2014; Mulitza et al., 2017). Yet, these models were not capable to capture the spatio-temporal complexity of HS1, which was revealed from high resolution paleo-reconstructions based on marine sediment archives showing a high internal climatic variability of HS1 (Bahr et al., 2018; Hodell et al., 2017).

Besides model evidence for an increase in SST in the tropical South Atlantic in response to weak AMOC, there is a fundamental lack of knowledge about the thermal response of the tropical western South Atlantic as there are no SST records available which adequately resolve the rapid climatic fluctuations during HS1. This is an important shortcoming as the tropical western South Atlantic is of vital importance for deciphering the mechanism leading to the bipolar distribution of oceanic heat during an AMOC slowdown. Here we present the first high-resolution foraminiferal Mg/Ca-based SST record covering the last deglacial from the tropical western South Atlantic. Our data reveal a pronounced anti-phased pattern between an extremely amplified heat transport by the BC and greatly diminished NBC transport resulting in a yet unrecognized extreme warming in the tropical western South Atlantic significantly exceeding model simulations.

2. Oceanographic Setting

The surface hydrography in the western South Atlantic is dominated by the southward-flowing BC carrying warm tropical waters from the bifurcation (10°S–15°S) of the Southern South Equatorial Current (SSEC) (Peterson & Stramma, 1991) (Figure 1). The BC flows southwards along the Brazilian margin as far as ~38°S where it converges with the northward-flowing cool Malvinas Current (MC) (Stramma & England, 1999) (Figure 1). At the Brazil-Malvinas confluence (BMC), the BC separates from the coast and flows eastward (Matano et al., 1993). The cooler Brazilian Coastal Current (BCC) emerges from the BMC and flows along the inner shelf in the opposite direction in relation to the BC. It is composed by a mixture of tropical BC and cool subantarctic MC waters (de Souza & Robinson, 2004). The present BCC influence reaches as far as 24°S and depends on southwestern wind strength (de Souza & Robinson, 2004). The northward-flowing NBC carries warm surface waters into the Northern Hemisphere. Between 7°N and 8°N, portions of the NBC are retroflected into the eastward flowing North Equatorial Countercurrent (NECC). It is noteworthy that the retroflection efficiency varied in the past and was likely stronger in glacial stages (Wilson et al., 2011). Waters of the NBC, which are not retroflected, flow northwestward finally reaching the Caribbean Sea. Importantly, a strong NBC is required to compensate for the formation and southward flow of North Atlantic Deep Water, thus the NBC appears to be especially sensitive to changes in AMOC strength and itself has the capacity to modulate high latitude deep water formation (Dahl et al., 2005; Fratantoni et al., 2000; Rühs et al., 2015; Zhang et al., 2011).

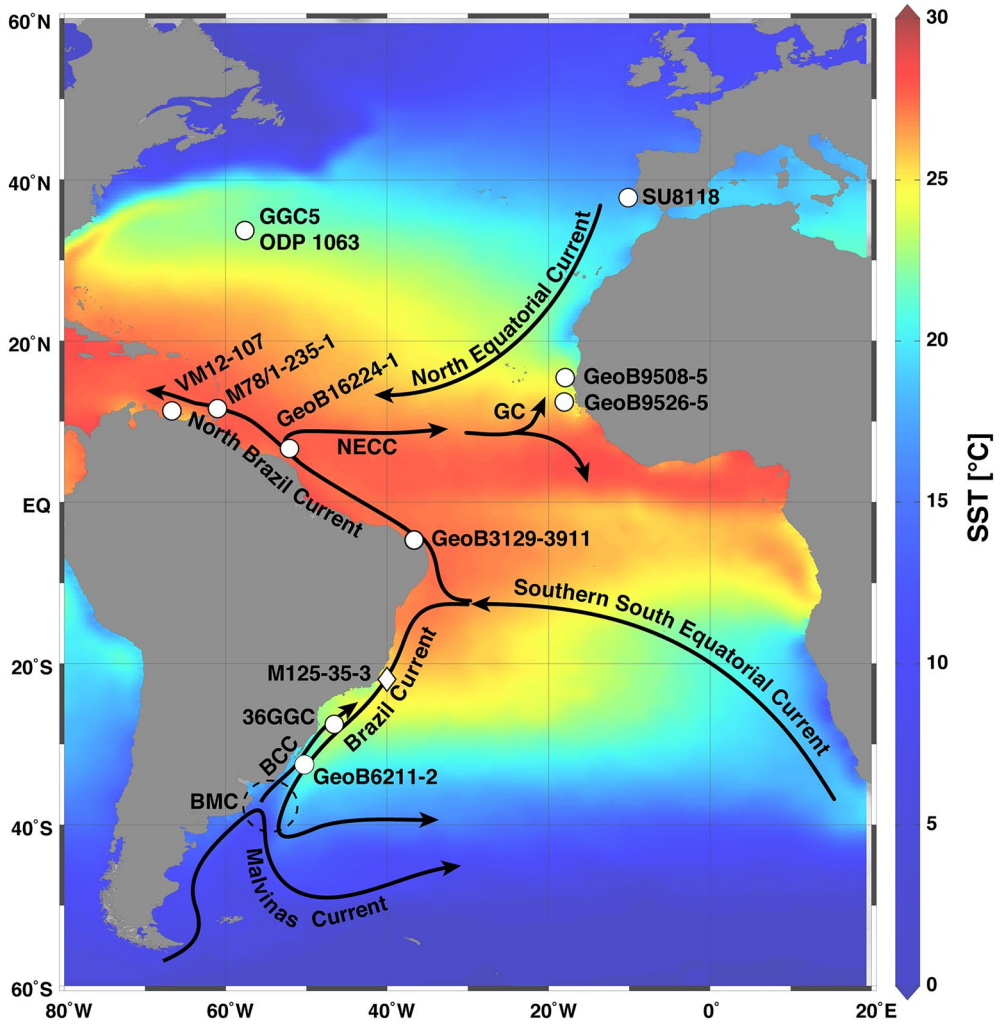

Figure 1. Hydrographic map of the Atlantic Ocean including surface currents. The color shading displays annual mean sea surface temperature (SST) (Locarnini et al., 2013). White diamond locates Core M125-35-3 (this study). White dots represent locations of previously published proxy-records mentioned in the text. Black dashed circle indicates the Brazil-Malvinas Confluence (BMC). BCC: Brazilian Coastal Current. NECC: North Equatorial Countercurrent. The modern Brazil Current is partially retroflected into the eastward-flowing NECC. GC: Guinea Current.

3. Materials and Methods

Gravity core M125-35-3 was retrieved from the continental shelf off SE Brazil (21°53.606′S, 040°00.279′W, 428.6 m water depth) during R/V Meteor cruise M125 in 2016 (Bahr et al., 2016). A total of 4.25 m of sediment was recovered. For geochemical analyses, the core was sampled between 25 and 170 cm at 1 cm spacing. All samples were wet-sieved over a 63 μm mesh, oven-dried at 40°C and subsequently dry-sieved over 355 and 400 μm meshes. Per sample, 50–60 specimens of the surface-dwelling foraminifera *Globigerinoides ruber* (pink variety) (Chiessi et al., 2007) were handpicked from the dried sediments under a stereo microscope. Based on data from a sediment-trap located off SE Brazil at 23.6°S, Venancio et al. (2017) inferred that *G. ruber* (p) is the best-suited planktonic foraminiferal species to reconstruct surface-ocean conditions in the western South Atlantic. During the interval sampled by the sediment trap, *G. ruber* (p) did not show any significant seasonal changes in its occurrence, reflecting annual mean conditions. The apparent calcification depth of *G. ruber* (p) at the site studied by Venancio et al. (2017) was determined as the mixed layer between 30 and 40 m water depth, which is similar to estimated calcification depth of *G. ruber* in the Pacific Ocean (Rippert et al., 2016) and slightly shallower than in the Indian Ocean (Stainbank et al., 2019). To avoid size-related ontogenic effects (Elderfield et al., 2002), foraminiferal tests were sampled from the

355–400 μm size fraction (Friedrich et al., 2012). Thereafter, foraminiferal tests were gently crushed between two glass plates to remove potential contamination by residual detrital sediments and expose the test chambers to subsequent chemical treatment. Only the cleanest test fragments were used for trace metal analysis. The chemical cleaning steps followed the cleaning protocol of Martin and Lea (2002), excluding an additional DTPA step (Weldeab et al., 2006). Mg/Ca analyses were carried out on a ThermoScientific™ Element 2 HR-ICP-MS at the Institute of Geosciences, Heidelberg University. The results were normalized to the external standard ECRM752-1 (3.762 mmol/mol Mg/Ca; Greaves et al., 2008), which was repeatedly measured after every sample to control potential instrumental drift. The external mean reproducibility for the ECRM752-1 was ±0.07 mmol/mol for Mg/Ca (2σ). An internal standard (indium) was added to stabilize matrix effects of the samples. The cleaning efficiency for foraminiferal tests of Core M125-35-3 was carefully monitored by measuring the diagnostic elements Mn, Fe, and Al to indicate potential Mn- and Fe-oxide enriched coatings, and clay mineral contamination, respectively. We provide details on the diagnostic elements in the supporting information (cf. supporting text S1 and Figure S1). SSTs were converted from Mg/Ca ratios using the species-specific equation for *G. ruber* (p) by Dekens et al. (2002) as they used core-tops from the tropical Atlantic. Details on stable oxygen isotope measurements are presented in supporting information (cf. supporting text S2 and Figure S2).

The age model for Core M125-35-3 was constrained by eight accelerator mass spectrometry AMS ^{14}C dates measured on the planktic foraminifera *G. ruber* (p). Three of the AMS ^{14}C datings were performed by BETA Analytics Limited in Miami (USA), the remaining five at LARA laboratory of the University of Bern (Switzerland). ^{14}C-ages were calibrated to cal kyr BP (in the following simplified as ka) using the Marine13 calibration curve (Reimer et al., 2013). We applied a local reservoir effect of $\Delta R = 85 \pm 25$ inferred from Alves et al. (2015) for the eastern tropical South American margin. The final age model was constrained using the CRAN *R* package Bacon (version 2.4.2), which uses Bayesian statistics to reconstruct Bayesian accumulation histories (Blaauw & Christen, 2011). We did not exclude the outlying AMS ^{14}C date obtained at 70.5 cm as the CRAN R-Bacon script uses a Student-*t* model to calibrate the AMS ^{14}C dates with wider tails of the calibration model. Hence, the age model is robust to the presence of outliers (Blaauw & Christen, 2011). The resulting age model (Figure 2 and Table 1) covers the target interval from 20 to 10 ka, comprising the latest part of the Last Glacial Maximum (LGM), HS1, the Bølling-Allerød interstadial, the Younger Dryas (YD), and the Early Holocene (EH). Sedimentation rates are varying from 6.5 to 17.6 cm/kyr and on average 12.8 cm/kyr corresponding to an averaged temporal resolution of 87 yr for our record. An interval of higher sedimentation rates occurs from ~13.8 to ~17.7 ka, resulting in an even higher temporal resolution of ~60 yr during HS1 (Figure 2).

4. Results and Discussion

4.1. BC Heat Transport Variability at Site M125-35-3 During the Last Deglaciation

Within the interval from the end of the LGM at 19.7 ka toward ~15.5 ka (i.e., late HS1), the M125-35-3 $SST_{Mg/Ca}$ record reveals a distinctive high-amplitude variability of $SST_{Mg/Ca}$ (Figure 3). A general warming trend during this interval is intermitted by rapidly occurring cool phases centered at ~18.5 and ~17 ka with $SST_{Mg/Ca}$ as low as 20°C. During HS1 at 16 ka, $SST_{Mg/Ca}$ reach a prominent maximum of ~32°C which is coinciding with the IRD peak of Core SU8118 (Bard et al., 2000) indicating HE1a (Figure 5). We note that the peak SST of ~32°C during deglacial boundary conditions is likely overestimated due to the positive effects of increased surface salinity (which would be expected to occur together with increased SST) on the incorporation of Mg in foraminiferal calcite (Gray & Evans, 2019; Hönisch et al., 2013). To assess the potential effect of salinity changes on SST estimates, we calculated sea-surface salinity combining δ^{18}O and Mg/Ca measurements on *G. ruber* (p) (see supporting information Text S2 and Figure S2 for further details). We note that this approach will overestimate the salinity anomaly due to the positive influence of salinity on Mg/Ca. Based on these estimates, we conclude that the salinity difference between present-day conditions of 36.83 g/kg (Locarnini et al., 2018), and the SST peak at 16 ka amounts to 0.95–1.36 g/kg. Such an increase in salinity could result in an anomalous SST increase of 1.4°C if one considers a Mg/Ca change of *G. ruber* by 3.3% per salinity unit (Hönisch et al., 2013). By including the error propagation of Mg/Ca-derived SSTs in the order of 1°C (Mohtadi et al., 2014) to the salinity effect, we suggest that the maximum overestimation of peak SST to be 2.4°C. Thus, the salinity-corrected SST peak is 29.6°C at 16 ka, which is still corroborating a

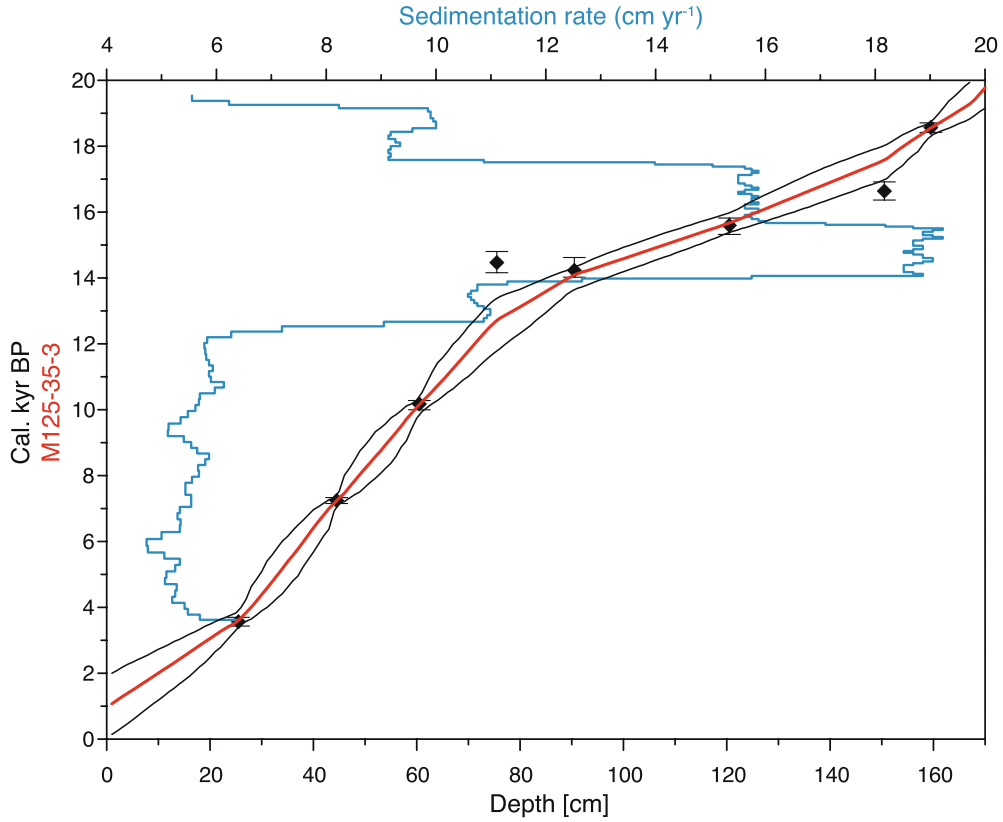

Figure 2. Age model and sedimentation rate of sediment Core M125-35-3. The red thick line illustrates the median age probabilities modeled with Bacon, which is used to construct the age model of Core M125-35-3. The black lines indicate maximum and minimum age 2σ probabilities for the model outcome. Black diamonds illustrate AMS ^{14}C-dates for Core M125-35-3 including error bars. The blue line indicates sedimentation rate.

strong warming by at least 4.6°C during HS1a at Core M125-35-3. After HE1a, $SST_{Mg/Ca}$ drops to 26°C at the onset of the Bølling/Allerød and increases gradually to ~30°C during the YD with the exception of a short ~3°C cooling during the early YD (Figure 3). During the EH from 11. 7 ka to the end of the record at 10 ka, $SST_{Mg/Ca}$ become slightly colder again with values around 27°C.

Table 1
Calibrated AMS ^{14}C Ages Measured on the Planktonic Foraminifera G. ruber Pink Using the Calib 7.1 Software and the MARINE13 Calibration Curve With ΔR = 85 ± 25

Depth (cm)	Lab code	^{14}C age BP (years)	Error of ^{14}C ages (years)	Calibrated median age (years)
25.5	BE-7261.1.1	3,743	±42	3,564
44.5	Beta-530016	6,800	±30	7,245
60.5	BE-7267.1.1	9,414	±43	10,172
75.5	Beta-530017	12,890	±40	14,467
90.5	BE-7268.1.1	12,781	±52	14,231
120.5	BE-7269.1.1	13,516	±54	15,596
150.5	BE-72701.1	14,254	±59	16,636
159.5	Beta530018	15,780	±40	18,567

To assess the heat distribution in the tropical western South Atlantic and its modulation by the BC during the last deglaciation, we compared the $SST_{Mg/Ca}$ record of M125-35-3 with the southerly located subtropical high-resolution $SST_{Mg/Ca}$ record of sediment core GeoB6211-2 (Chiessi et al., 2015). This core was collected at 32.5°S off southern Brazil and, thus, within the flow path of the BC (Figure 1). The modern difference between SSTs of cores M125-35-3 and GeoB6211-2 varies according to the season and show an annual average of 4.1°C (Locarnini et al., 2013). Both $SST_{Mg/Ca}$ records reveal broadly similar trends, however, with two marked deviations. First, between ca. 20 and 16 ka, $SST_{Mg/Ca}$ fluctuations at Site M125-35-3 are much more pronounced than in GeoB6211-2. Second, during the $SST_{Mg/Ca}$ maximum of M125-35-3 at ~16 ka, the GeoB6211-2 record shows a diverging cooling trend (Figure 2). We interpret the high $SST_{Mg/Ca}$ variability during the late LGM and HS1 at Site M125-35-3 to be caused by transient northward intrusions of the BCC, carrying portions of cool subantarctic waters toward Site M125-35-3. This is in line with dinocyst assemblages from Core GeoB6211-2 which indicate that the BCC had a noticeable influence on this site until ca. 15 ka (Gu et al., 2018). The

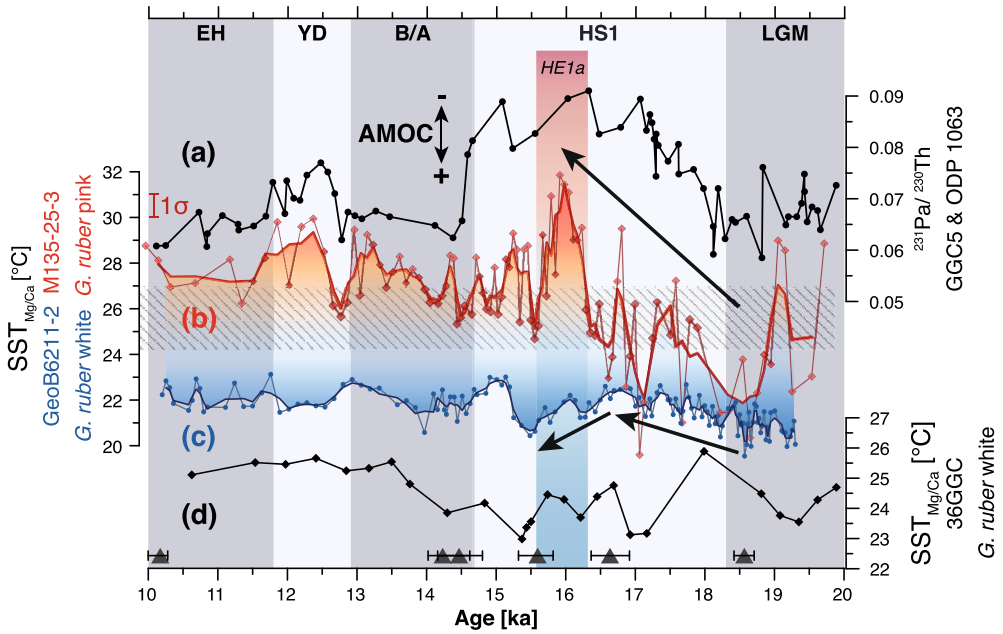

Figure 3. Mg/Ca based sea surface temperatures ($SST_{Mg/Ca}$) records from the tropical- and subtropical South Atlantic across the last deglaciation. (a) $^{231}Pa/^{230}Th$ compilation from Core GGC5 and ODP Site 1063 representing Atlantic Meridional Overturning Circulation strength (Böhm et al., 2015; Lippold et al., 2019; McManus et al., 2004). (b) $SST_{Mg/Ca}$ record of Core M125-35-3 (this study) with 3-point running average (thick red line). The hatched area indicates modern annual SST at Core M125-35-3. 1σ represents the error propagation of 1°C resulting from the calibration uncertainties after converting Mg/Ca ratios to SSTs as calculated by Mohtadi et al. (2014). (c) $SST_{Mg/Ca}$ record of GeoB6211-2 (Chiessi et al., 2015) with 3-point running average (dark blue line). (d) $SST_{Mg/Ca}$ record of 36GGC (black) (Carlson et al., 2008). Triangles represent AMS ^{14}C datings of Core M125-35-3. LGM: Last Glacial Maximum. HS1: Heinrich Stadial 1. HE1a: Heinrich Event 1a. B/A: Bølling-Allerød interstadial, YD: Younger Dryas. EH: Early Holocene.

short-term prevalence of the BCC at M125-35-3, particularly during the cold spells at 18.5 and 17 ka, was likely fostered by the lower sea level that shifted the BCC offshore toward the upper continental slope, hence more proximal to Core M125-35-3. We cannot fully exclude a putative cooling effect of increased coastal upwelling, especially at the Cabo Frio region which is close to the location of Core M125-35-3. However, a reconstruction of upwelling variability in close vicinity to Core M125-35-3 revealed significantly decreased coastal upwelling during the last 20.0 ka (Portilho-Ramos et al., 2015). Coastal upwelling along the south Brazilian margin is induced by strengthened northeasterly winds, which would be further in conflict with an enhanced northward intrusion of BCC waters (Gu et al., 2018). Thus, we argue that upwelling only affected the SST record of Core M125-35-3 to a minor degree. The pronounced warm event in Core M125-35-3 during HE1a at 16 ka on the other hand is not evidenced in GeoB6211-2 $SST_{Mg/Ca}$, indicating that the latter site was still under the influence of the BCC in contrast to Core M125-35-3 which was fully bathed by the BC. This implicates the generation of a steep hydrographic front between both sites, which likely resulted from the strongly altered trade wind pattern during HE1a. Despite the lower temporal resolution, another Mg/Ca-based SST record (Core 36GGC) (Figures 1 and 3) from the Brazilian margin from 27.5°S shows some similarity with the GeoB6211-2 record (Chiessi et al., 2015), indicating that the frontal system must have developed between cores M125-35-3 and 36GGC.

Freshwater hosing experiments simulating HS1 suggest distinct spatial shifts of the trade winds across the South Atlantic in response to a southward shift of the ITCZ resulting in southeast-ward surface wind anomalies in the tropical South Atlantic (Figure 4) (McGee et al., 2018). We, therefore, assume that due to increased eastward wind stress and Ekman transport, the BC may have separated earlier (i.e., in lower latitudes) from the South American coast than compared to today and only a minor fraction of BC waters has been admixed to the BCC. The relative decrease in BC waters which are admixed to the BCC would also explain the diverging cooling trend at Core GeoB6211-2 during HE1a. Additionally, the model data suggest

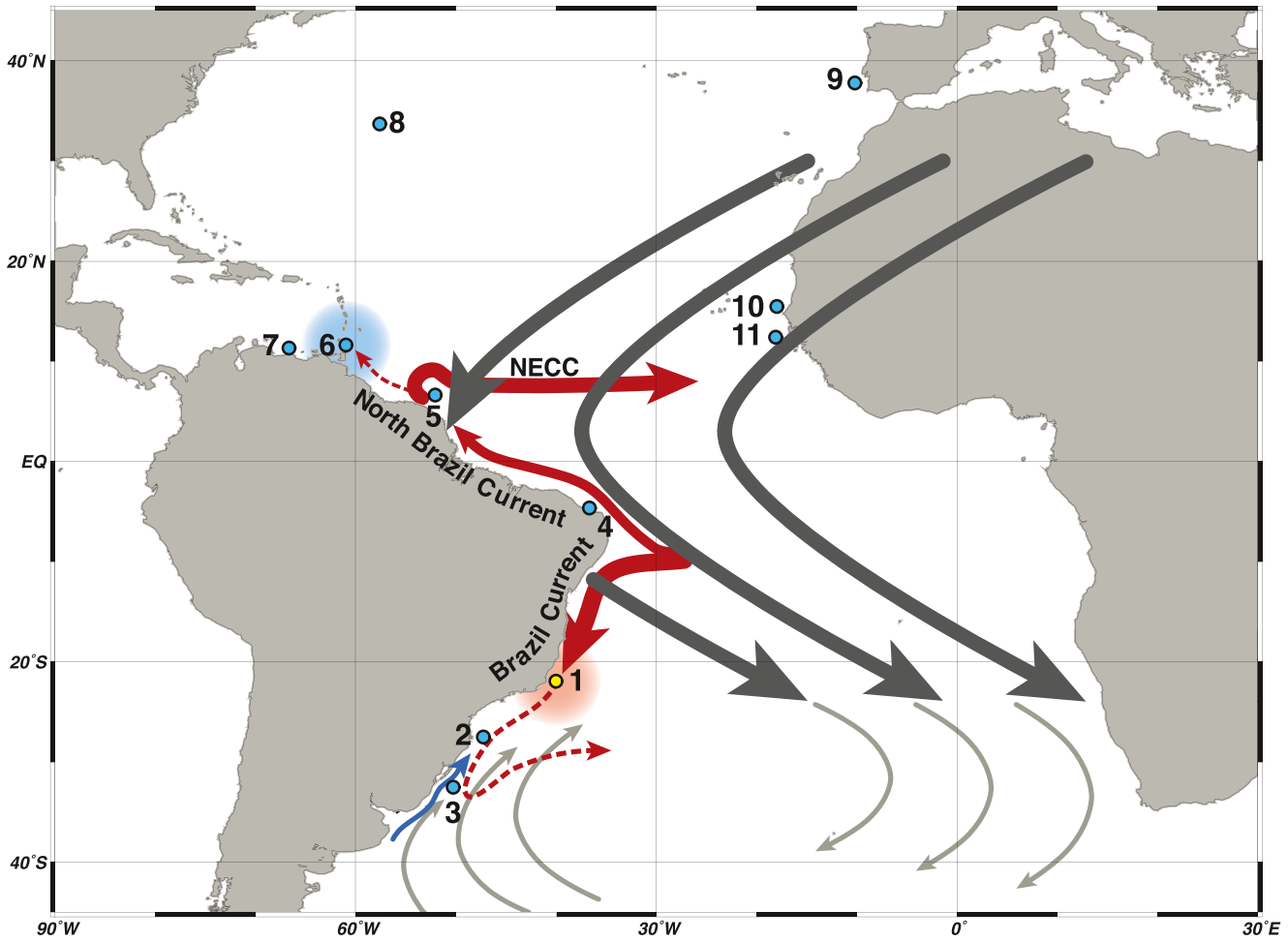

Figure 4. Scheme of anomalously altered wind pattern and corresponding oceanic surface currents during Heinrich Stadial 1 (HS1) after McGee et al. (2018) and core locations mentioned in the main text. Thick red arrows illustrate warm tropical Brazil Current, North Brazil Current, and North Equatorial Countercurrent (NECC). Thick gray arrows indicate the wind anomaly during HS1. The dashed red lines represent diminished southward and northwestward-flow of warm waters by the Brazil Current and North Brazil Current respectively. Blue arrow indicates northward flow of the cold Brazil Coastal Current (BCC). NECC: North Equatorial Counter Current. (1) M125-35-3 (this study) with red shading indicating sea surface warming during HS1, (2) 36GGC (Carlson et al., 2008), (3) GeoB6211-2 (Chiessi et al., 2015), (4) GeoB3129-3911 (Weldeab et al., 2006), (5) GeoB16224-1 (Crivellari et al., 2018), (6) M78/1-235-1 (Bahr et al., 2018), blue shading indicates cooling at this site, (7) VM12-107 (Schmidt et al., 2012), (8) GGC5 (McManus et al., 2004), (9) SU8118 (Bard et al., 2000), (10) GeoB9526-5, (11) GeoB9526-5 (Zarriess et al., 2011).

a cyclonic wind pattern arising in the southwest South Atlantic between ~20 and 35°S leading to northward coastal surface winds along eastern South America. The northward wind component may have forced enhanced northward flow of cooler subantarctic waters carried by the BCC countering the southward heat advection by the BC (Figure 4). The persistently high $SST_{Mg/Ca}$ >24°C at Site M125-35-3 after 15 ka and the establishment of a constant SST gradient to Site GeoB6211-2 which is close to modern (Figure 3) argues for a prevalence of the BC at both sites from 15 ka onwards, supported by the occurrence of typical BC dinocyst assemblages at GeoB6211-2 (Gu et al., 2018).

4.2. The NBC-BC Seesaw

The BC has been suggested to redirect excess heat into the South Atlantic in times of AMOC slowdown (Chiessi et al., 2015; Crowley, 1992; Maier-Reimer et al., 1990). Thus, we would expect increased $SST_{Mg/Ca}$ at Site M125-35-3 caused by AMOC slowdowns such as during HS1. Indeed, the good correlation between $^{231}Pa/^{230}Th$ from cores GGC5 and ODP Site 1063 (Böhm et al., 2015; Lippold et al., 2019; McManus et al., 2004) (Figure 1), indicating changes in AMOC strength, and the M125-35-3 $SST_{Mg/Ca}$ record supports

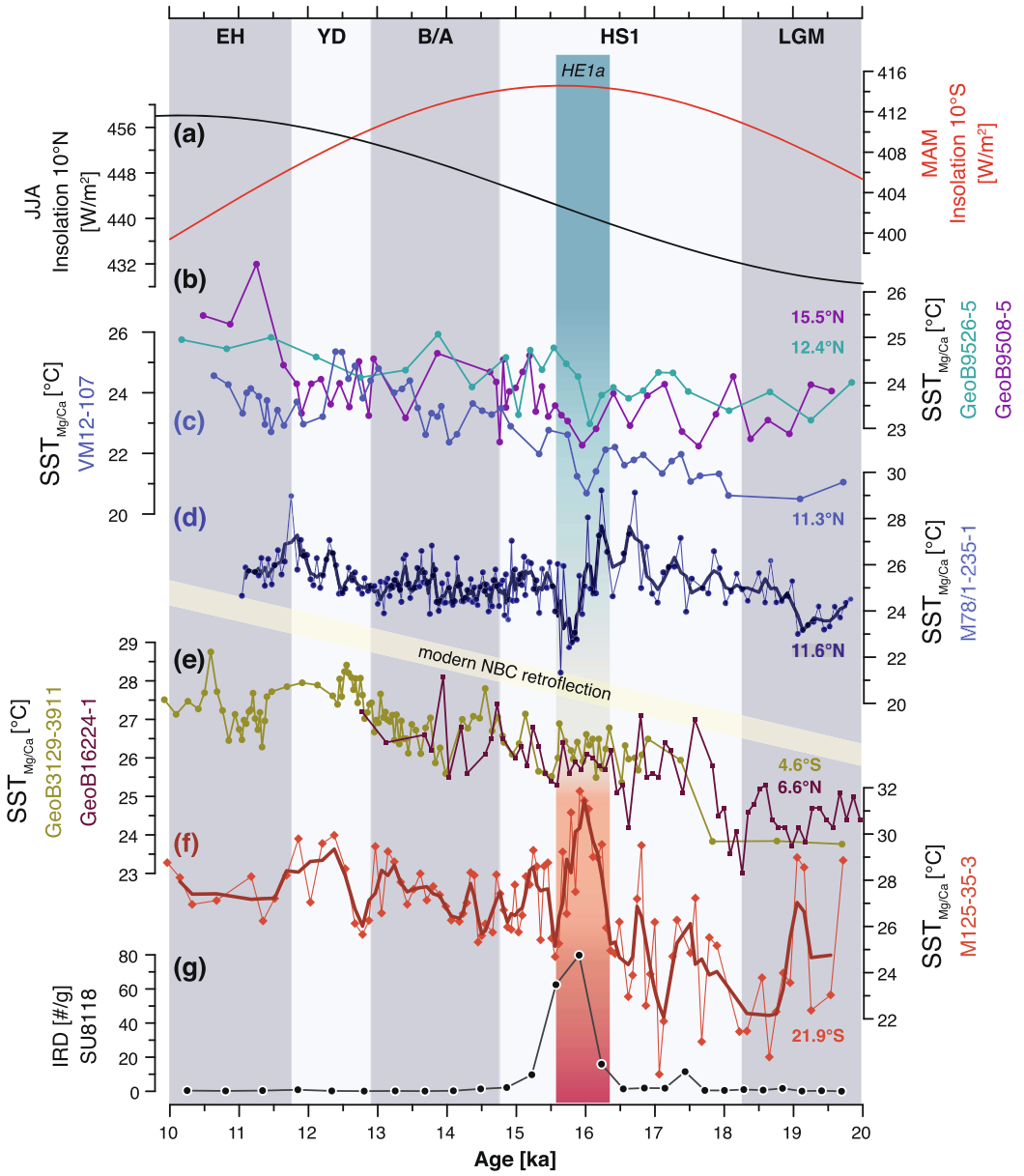

Figure 5. Correlation of proxy-records based on marine sediment cores from the Atlantic Ocean during the last deglaciation. (a) Mean austral autumn insolation (March to May) at 10°S (red) and mean boreal summer insolation (June to August) at 10°N (Laskar et al., 2004). (b) Mg/Ca based sea surface temperature ($SST_{Mg/Ca}$) records of cores GeoB9526-5 and GeoB9508-5 from the tropical eastern North Atlantic (Zarriess et al., 2011). (c) $SST_{Mg/Ca}$ record of Core VM12-107 located in the Bonair Basin (Schmidt et al., 2012). (d–f) $SST_{Mg/Ca}$ transect along the western South American margin. (d) $SST_{Mg/Ca}$ record of Core M78/1-235-1 (Bahr et al., 2018) located at 11.6°N representing the northern endmember of the North Brazil Current (NBC), thick line denotes 3-point running average; (e) $SST_{Mg/Ca}$ records south of the modern NBC retroflection from GeoB16224-1 (6.7°N) (Crivellari et al., 2018) and GeoB3129-3911 (4.6°S) (Weldeab et al., 2006). (f) $SST_{Mg/Ca}$ record of Core M125-35-3 (this study) with 3-point running average (thick red line) reflecting the southern part of the transect. (g) Ice-rafted detritus (IRD) record of Core SU8118 from the Iberian Margin (Bard et al., 2000). The yellow tilted band marks the boundary of cores located north and south of the modern NBC retroflection. LGM: Last Glacial Maximum. HS1: Heinrich Stadial 1. HE1a: Heinrich Event 1. B/A: Bølling-Allerød Interstadial, YD: Younger Dryas. EH: Early Holocene.

the high sensitivity of the tropical Atlantic surface heat balance to AMOC variability (Figure 3). With the onset of AMOC slowdown at the beginning of HS1, $SST_{Mg/Ca}$ of M125-35-3 follows the gradual increase of $^{231}Pa/^{230}Th$ (AMOC slowdown) as displayed by a the warming trend between 18.5 and 16 ka. OHT by the BC was most efficient at 16 ka displayed by maximum M125-35-3 $SST_{Mg/Ca}$ of at least 29.6°C, coinciding with HE1a and the weakest AMOC (Figures 3 and 5). However, the pronounced SST fluctuations around 16 ka are not mimicked by $^{231}Pa/^{230}Th$ fluctuations, pointing at additional factors besides AMOC strength influencing SST variability (see below). Heat accumulation by the BC ceased rapidly after 16 ka and with the recovery of the AMOC at the onset of the Bølling-Allerød interstadial (~14.5 ka), the subsequent long-term trend of the M125-35-3 $SST_{Mg/Ca}$ record noticeably parallels the $^{231}Pa/^{230}Th$ record throughout the Bølling-Allerød, YD, and EH (Figure 3). A short SST drop of about ~3°C in Core M125-35-3 at around 12.9 ka appears to coincide with the AMOC slow-down at the onset of the YD (e.g., Lynch-Stieglitz 2011; Muschitiello et al., 2019; Thornalley et al., 2011), which would imply warming at our study site by reduced northward heat transport. However, we note that the age-model uncertainty of Core M125-35-3 around this time interval does not allow to constrain the exact timing of this short-lived cooling event which might well pre-date the onset of the YD. Considering these caveats, the long-term trends of both, Core M125-35-3 $SST_{Mg/Ca}$ and the $^{231}Pa/^{230}Th$ AMOC reconstruction, are consistent and salient patterns that point at AMOC essentially driving the heat transport by the BC during the last deglaciation.

It has been argued that enhanced transport of oceanic heat into the South Atlantic during HS1 and the YD was facilitated by a weakening of the NBC reducing the advection of warm waters into the Northern Hemisphere (e.g., Rühs et al., 2015; Zhang et al., 2011) leading to an anti-phased pattern between the BC and the NBC (Arz et al., 1998, 1999). To reconstruct the potential mechanism involved in an anti-phased BC-NBC pattern and the spatio-temporal variability of the northward directed heat transport, we compiled a N-S transect of $SST_{Mg/Ca}$ records with sufficiently high-resolution during HS1 along the eastern South American continental margin (Figures 1 and 5). We use the $SST_{Mg/Ca}$ record of M78/1-235-1 (11.6°N) (Bahr et al., 2018) as an end-member for net northward heat transport, as NBC waters may partially recirculate into the tropical Atlantic (Wang et al., 2004; Wilson et al., 2011) (Figure 1). In contrast, GeoB3129-3911 (4.6°N) (Weldeab et al., 2006) and GeoB16224-1 (6.7°S) (Crivellari et al., 2018) are located to the south of the modern retroflection area of the NBC (Figure 1). This meridional differentiation between core sites north or south of the retroflection is instrumental when assessing the NBC as the main pathway for the northward cross-equatorial OHT and hence, the interhemispheric heat balance (Arz et al., 1998; Rühs et al., 2015; Wang et al., 2004). The comparison of those records reveals one marked interval of apparent anti-phased evolution of the BC and NBC during the last deglaciation, namely the marked SST increase of 7°C during HE1a in the M125-35-3 record which is within age model uncertainties (Figure 6) concomitant with a rapid ~6°C SST cooling in the M78/1-235-1 record (Bahr et al., 2018; Reiβig et al., 2019). To test the robustness of the concurrency of these thermal events, we reassessed the existing age model of Core M78/1-235-1 (Reiβig et al., 2019) by using the CRAN *R* Bacon package implementing the published AMS ^{14}C data and reservoir correction ($\Delta R = -27 \pm 1$) as applied by Reiβig et al. (2019). We correlated our $SST_{Mg/Ca}$ record of Core M125-35-3 with the M78/1-235-1 record, illustrated as "Ghost Plots" provided by Bacon (Blaauw & Christen, 2011) which indicates the $SST_{Mg/Ca}$ record with its Monte Carlo-based age model uncertainties (Figure 6). The data reveal that the cooling at Core M78/1-235-3 during HE1a was likely to happen in coincidence with the warming at Core M125-35-3 peaking at 16 ka. This temporal coincidence is further supported by a $SST_{Mg/Ca}$ minimum during HE1a in Core VM12-107 (Schmidt et al., 2012) collected from the Bonaire Basin, upstream of M78/1-235-1. The $SST_{Mg/Ca}$ minimum in VM12-107 also occurs at 16.0 ka, being therefore synchronous to the M125-35-3 $SST_{Mg/Ca}$ maximum during HE1a (Figure 5).

Notably, the GeoB3129-3911 and GeoB16224-1 records south of the NBC retroflection are both characterized by constant SSTs during HE1a. On the basis of this spatial SST pattern, we propose the following oceanographic configuration for HE1a: Heat transport by the BC was considerably intensified while the NBC flow was active at least up to 6.7°N (i.e., the latitude of GeoB16224-1). A strong retroflection apparently prevented a cross-equatorial flow of the NBC, evidenced in the distinct cooling at Core M78/1-235-1. HS1 model simulations further show that in line with a southward shift of the ITCZ, equatorial near-surface winds in the low latitudes off northeastern South America show an anomalous strengthening in the opposite direction relative to the NBC flow-direction (McGee et al., 2018). This atmospheric forcing may have substantially weakened the NBC, finally resulting in a diminished northwestward flow. However, as there is a persistent

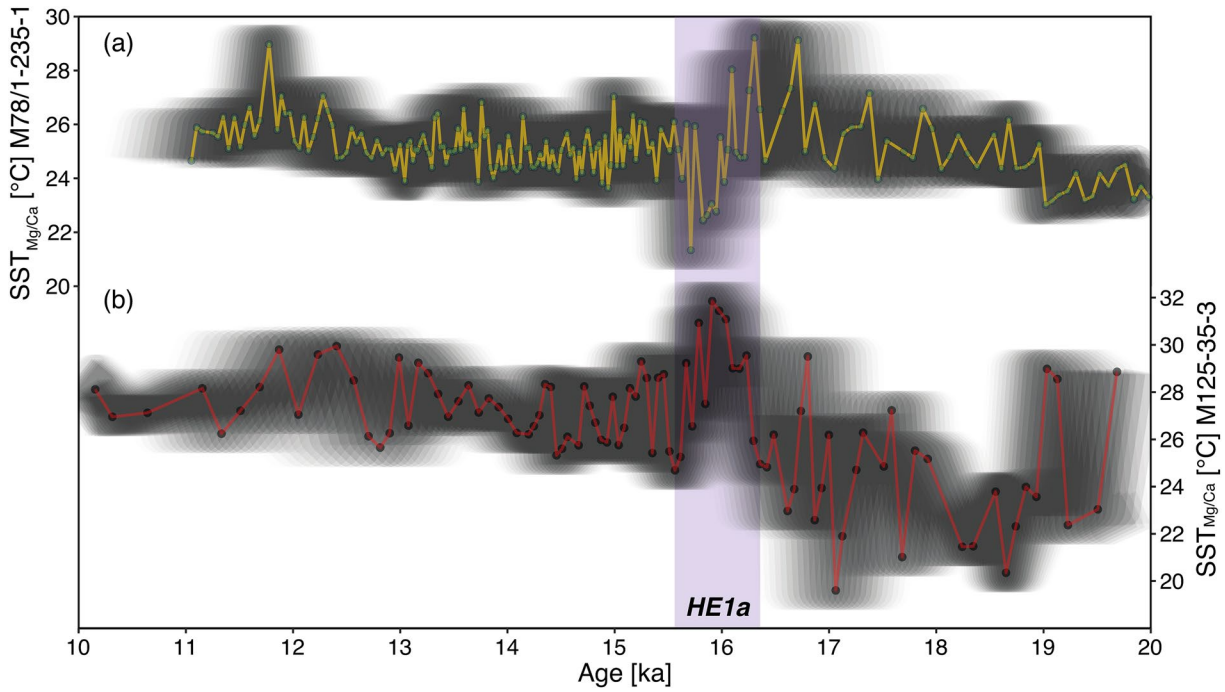

Figure 6. "Ghost Plot" correlation of the $SST_{Mg/Ca}$ records of cores M78/1-235-1 and M125-35-3. (a) M78/1-235-1 $SST_{Mg/Ca}$ Ghost Plot. The yellow line indicates the $SST_{Mg/Ca}$ record of Core M78/1-235-1 (Bahr et al., 2018) vs. the median age model outcome by Bacon (Blaauw & Christen, 2011) based on the chronostratigraphy of Reiβig et al. (2019). The grayscale indicates minimum and maximum age probabilities from the Bacon age model outcome where darker gray indicates high probabilities and lighter gray low probabilities. (b) Ghostplot of the $SST_{Mg/Ca}$ record of Core M125-35-3 (this study). Thick red line indicates $SST_{Mg/Ca}$ of Core M125-35-3 versus median age. Purple shaded area indicates Heinrich Event 1 (HE1a) including the timing of coincident warming (cooling) at Core M125-35-3 (M78/1-235-1) at 16 ka.

NBC flow at least up to 6.7°N, we do not claim for a full reversal of the NBC, which is in agreement with Zhang et al. (2015). Rather, we assume a strengthened retroflection of the NBC into the NECC north of 6.6°N, which is also supported by Wilson et al. (2011). Indeed, these authors found evidence for a prolonged retroflection of the NBC forced by the trade wind pattern emerging during the southward shift of the ITCZ. The extreme southward displacement of the ITCZ during HE1a was further fostered by the insolation configuration with maximal austral autumn (March-May) insolation occurring at ~16 ka parallel to relatively low boreal summer insolation (Figure 5), further heating the southern relative to the Northern Hemisphere. The insolation maximum may also have contributed to the very warm SSTs during HE1a recorded in Core M125-35-3. The warming of tropical waters carried by the BC was likely favored by the general slowdown of the AMOC and weak Southern Hemisphere trade winds during Northern Hemisphere cold phases, leading to a slowdown of the South Atlantic subtropical gyre and thus, to a sluggish BC. This may have promoted radiative warming of tropical waters carried by the BC on its way to Core M125-35-3. The decreased export of warm waters via the NBC to the Northern Hemisphere, together with the increased recirculation of warm waters within the South Atlantic, further contributed to the evolution of a warm pool in the western tropical South Atlantic leading to extensive warming of the BC as seen at 16.0 ka in our SST record. Interestingly, we do not find a HE1a-like BC-NBC anti-phase during the YD which is as well an interval of strong Northern (Southern) Hemisphere cooling (warming) and AMOC slowdown (Barker et al., 2009). The YD was, however, not characterized by such extreme HS1-like AMOC perturbations as inferred from the $^{231}Pa/^{230}Th$ data (Figure 3) and the insolation forcing during austral summer/autumn was lower (Figures 3 and 5). As a result, the ITCZ did not occupy such an extreme southward position as during HS1 (Mulitza et al., 2017) and trade wind patterns were not as profoundly altered. Thus, we argue that the combined mechanism of extreme AMOC slowdown and maximum austral autumn insolation resulted in an extreme southward shift of the ITCZ during HS1 in line with substantially increased (decreased) Northern (Southern) Hemisphere trade winds. We suggest that besides the AMOC slowdown at 16 ka, the pronounced anti-phased tropical Atlantic SST pattern between the BC and the NBC (as recorded in the SST records of cores M125-35-3 and

M78/1-235-1, respectively) was markedly amplified by the effect of an atmospheric teleconnection triggered by the altered trade wind circulation around 16 ka (cf. Figure 4).

4.3. Implications for the Meridional Heat Transport During Phases of Weak AMOC

Fresh water hosing model experiments for HS1 commonly show that sea-surface warming in the tropical and subtropical South Atlantic occurred after a reduction of AMOC heat transport by at least 75% (Chang et al., 2008; Dahl et al., 2005; Deplazes et al., 2013; Vellinga & Wu, 2008; Zhang & Delworth, 2005). However, the models imply a maximum warming anomaly of ~2°C while the salinity-corrected $SST_{Mg/Ca}$ amplitude of at least 4.6°C at Core M125-35-3 is more than two times as high. The high amplitude of surface warming in the tropical South Atlantic thus suggests that northward OHT was less efficient as predicted by numerical models in response to a severe AMOC reduction. The meridional SST transect from the western tropical Atlantic (Figure 5) demonstrates that, at least in the surface layer, a northward OHT into the North Atlantic via the NBC was almost absent. An alternative pathway for tropical-derived warm waters into the North Atlantic Ocean could be the Guinea Current at the west African coast (Figure 1), which is fed by the NECC carrying the retroflected waters of the NBC (Talley et al., 2011). Available data, however, argue against heat being advected along this pathway, as two planktic foraminiferal $SST_{Mg/Ca}$ records, GeoB9526-5 and GeoB9508-5, from the west African margin show distinct SST cooling at 16 ka (Zarriess et al., 2011) (Figures 1 and 5). The observed discrepancy between proxy data and numerical models might derive from both, (i) limitations of the models to resolve the spatio-temporal variability of complex features like western boundary currents such as the BC, as well as (ii) the shortage of proxy records with high temporal resolution from those critical oceanographic regions. The reliable assessment of the OHT during phases of sluggish AMOC (such as during HE1a), however, is a crucial aspect, as the interhemispheric heat imbalance arising from strongly reduced OHT must be compensated by enhanced cross-equatorial energy transport, which is primarily accomplished by meridional AHT (Cheng et al., 2013; Donohoe et al., 2012; Fasullo & Trenberth, 2008; McGee et al., 2018). Thereby, increased AHT is achieved by a southward shift and an invigoration of the Northern Hemispheric Hadley-Cell. This in turn, leads to the southward shift of the ITCZ and anomalously intensified NE trade winds (i.e., the lower branch of the Hadley-Cell) (Bjerknes, 1964; Yang et al., 2017), severely affecting hydroclimate in both (sub)tropical South America and Africa (e.g., Cruz et al., 2009; McGee et al., 2014; Stríkis et al., 2015). In light of a potential weakening of the AMOC in response to future global warming (Pachauri et al., 2014), it is thus essential to reliably quantify the associated ocean-atmosphere feedbacks. This demonstrates the urgent need of further improving the skill of high-resolution ocean models as well as the demand for a dense network of temporally highly resolved proxy-records from regions that are crucial for the cross-equatorial OHT and AHT respectively, such as the western tropical South Atlantic.

5. Conclusions

Our $SST_{Mg/Ca}$ record of Core M125-35-3 is the first SST record from the tropical South Atlantic adequately resolving the internal structure of HS1. We found evidence for a highly variable heat transport by the BC during the LGM and HS1, when the BC heat transport at Core M125-35-3 was frequently affected by northward intrusions of colder BCC-derived water masses. A modern-like BC evolved from late HS1 onwards. Extreme boundary conditions during HS1 (sluggish AMOC, maximum austral autumn and low boreal summer insolation) resulted in an anomalous southward shift of the ITCZ. Associated modifications of the trade winds led to a profound reorganization of the surface hydrography in the western tropical Atlantic. These changes caused an abrupt warming of at least 4.6°C at Core M125-35-3 at HE1a reflecting a highly efficient southward heat transport of the BC. We further find a seesaw-like pattern between a diminished capability of heat transport by the NBC and an increased efficiency in heat transport by the BC during HE1a, implying a near-collapse of the northward OHT, mostly owing to a strong retroflection of the NBC. The timing of this event at ~16 ka concurs with the most intense phase of iceberg discharge during HS1 (i.e., HE1a) and the almost complete shutdown of the AMOC. These findings further stress the importance of the NBC/BC system as a bottleneck of the AMOC return flow in the tropical Atlantic.

Data Availability Statement

All data will be made available in the Pangaea database https://doi.org/10.1594/PANGAEA.930612.

Acknowledgments
The authors kindly acknowledge the captain and crew of R/V METEOR during research cruise M125. Further, the authors thank Stefan Rheinberger for assistance in ICP-MS measurements, Swaantje Brzelinski and Oliver A. Kern for scientific discussion, Julia Hoffmann and Barbara Hennrich for laboratory assistance. The authors thank U. Röhl (editor) and two anonymous reviewers for constructive comments on our manuscript. AB acknowledges funding by the Deutsche Forschungsgemeinschaft (DFG Projects HO 5927/1-1, BA 3809/14-1). CMC acknowledges the financial support from FAPESP (grants 2018/15,123-4 and 2019/24,349-9), CAPES (grants 564/2015 and 88,881.313535/2019-01), CNPq (grants 422255/2016-5 and 312458/2020-7) and the Alexander von Humboldt Foundation. ALSA acknowledges CAPES-PRINT CLIMATE Project (grant 88,887.310301/2018-00), CAPES-ASpECTO project (grant 88,887.091731/2014-01) and CNPq (grant 302521/2017-8). JR acknowledges funding from the Focus Program of the Goethe University Frankfurt. Open access funding enabled and organized by Projekt DEAL.

References

Alves, E., Macario, K., Souza, R., Pimenta, A., Douka, K., Oliveira, F., et al. (2015). Radiocarbon reservoir corrections on the Brazilian coast from pre-bomb marine shells. *Quaternary Geochronology*, *29*, 30–35. https://doi.org/10.1016/j.quageo.2015.05.006

Arz, H. W., Pätzold, J., & Wefer, G. (1998). Correlated millennial-scale Changes in surface hydrography and terrigenous sediment yield inferred from last-glacial marine deposits off northeastern Brazil. *Quaternary Research*, *50*(2), 157–166. https://doi.org/10.1006/qres.1998.1992

Arz, H. W., Pätzold, J., & Wefer, G. (1999). The deglacial history of the western tropical Atlantic as inferred from high-resolution stable isotope records off northeastern Brazil. *Earth and Planetary Science Letters*, *167*(1–2), 105–117. https://doi.org/10.1016/S0012-821X(99)00025-4

Bahr, A., Hoffmann, J., Schönfeld, J., Schmidt, M. W., Nürnberg, D., Batenburg, S. J., & Voigt, S. (2018). Low-latitude expressions of high-latitude forcing during Heinrich Stadial 1 and the Younger Dryas in northern South America. *Global and Planetary Change*, *160*, 1–9. https://doi.org/10.1016/j.gloplacha.2017.11.008

Bahr, A., Spadano Albuquerque, A. L., Ardenghi, N., Batenburg, S., Bayer, M., Catunda, M. C., et al. (2016). *South American Hydrological Balance and Paleoceanography during the Late Pleistocene and Holocene (SAMBA) - Cruise No. M125 - March 21 - April 15, 2016 - Rio de Janeiro (Brazil) - Fortaleza (Brazil)*. Bremen: DFG-Senatskommission für Ozeanographie. https://doi.org/10.2312/cr_m125

Bard, E., Rostek, F., Turon, J.-L., & Gendreau, S. (2000). Hydrological impact of Heinrich events in the subtropical Northeast Atlantic. *Science*, *289*(5483), 1321–1324. https://doi.org/10.1126/science.289.5483.1321

Barker, S., Diz, P., Vautravers, M. J., Pike, J., Knorr, G., Hall, I. R., & Broecker, W. S. (2009). Interhemispheric Atlantic seesaw response during the last deglaciation. *Nature*, *457*(7233), 1097–1102. https://doi.org/10.1038/nature07770

Bjerknes, J. (1964). Atlantic air-sea interaction. In H. E. Landsberg, & J. Van Mieghem (Eds.), Eds., Advances in geophysics (Vol. 10, pp. 1–82). Elsevier. https://doi.org/10.1016/S0065-2687(08)60005-9

Blaauw, M., & Christen, J. A. (2011). Flexible paleoclimate age-depth models using an autoregressive gamma process. *Bayesian Analysis*, *6*(3), 457–474. https://doi.org/10.1214/11-BA61810.1214/ba/1339616472

Böhm, E., Lippold, J., Gutjahr, M., Frank, M., Blaser, P., Antz, B., et al. (2015). Strong and deep Atlantic meridional overturning circulation during the last glacial cycle. *Nature*, *517*(7532), 73–76. https://doi.org/10.1038/nature14059

Bond, G., Heinrich, H., Broecker, W., Labeyrie, L., McManus, J., Andrews, J., et al. (1992). Evidence for massive discharges of icebergs into the North Atlantic ocean during the last glacial period. *Nature*, *360*(6401), 245–249. https://doi.org/10.1038/360245a0

Broecker, W. S. (1998). Paleocean circulation during the last deglaciation: A bipolar seesaw? *Paleoceanography*, *13*(2), 119–121. https://doi.org/10.1029/97PA03707

Carlson, A. E., Oppo, D. W., Came, R. E., LeGrande, A. N., Keigwin, L. D., & Curry, W. B. (2008). Subtropical Atlantic salinity variability and Atlantic meridional circulation during the last deglaciation. *Geology*, *36*(12), 991–994. https://doi.org/10.1130/G25080A.1

Chang, P., Zhang, R., Hazeleger, W., Wen, C., Wan, X., Ji, L., et al. (2008). Oceanic link between abrupt changes in the North Atlantic Ocean and the African monsoon. *Nature Geoscience*, *1*(7), 444–448. https://doi.org/10.1038/ngeo218

Cheng, W., Bitz, C. M., & Chiang, J. C. H. (2007). Adjustment of the global climate to an abrupt slowdown of the Atlantic meridional overturning circulation. In *ocean circulation: Mechanisms and impacts—past and future changes of meridional overturning* (pp. 295–313). American Geophysical Union (AGU). https://doi.org/10.1029/173GM19

Chiessi, C. M., Mulitza, S., Mollenhauer, G., Silva, J. B., Groeneveld, J., & Prange, M. (2015). Thermal evolution of the western South Atlantic and the adjacent continent during termination 1. *Climate of the Past*, *11*(6), 915–929. https://doi.org/10.5194/cp-11-915-2015

Chiessi, C. M., Ulrich, S., Mulitza, S., Pätzold, J., & Wefer, G. (2007). Signature of the Brazil-Malvinas confluence (Argentine Basin) in the isotopic composition of planktonic foraminifera from surface sediments. *Marine Micropaleontology*, *64*(1), 52–66. https://doi.org/10.1016/j.marmicro.2007.02.002

Crivellari, S., Chiessi, C. M., Kuhnert, H., Häggi, C., da Costa Portilho-Ramos, R., Zeng, J.-Y., et al. (2018). Increased Amazon freshwater discharge during late Heinrich Stadial 1. *Quaternary Science Reviews*, *181*, 144–155. https://doi.org/10.1016/j.quascirev.2017.12.005

Crowley, T. J. (1992). North Atlantic deep water cools the Southern Hemisphere. *Paleoceanography*, *7*(4), 489–497. https://doi.org/10.1029/92PA01058

Cruz, F. W., Vuille, M., Burns, S. J., Wang, X., Cheng, H., Werner, M., et al. (2009). Orbitally driven east-west antiphasing of South American precipitation. *Nature Geoscience*, *2*(3), 210–214. https://doi.org/10.1038/ngeo444

Dahl, K. A., Broccoli, A. J., & Stouffer, R. J. (2005). Assessing the role of North Atlantic freshwater forcing in millennial scale climate variability: A tropical Atlantic perspective. *Climate Dynamics*, *24*(4), 325–346. https://doi.org/10.1007/s00382-004-0499-5

de Souza, R. B., & Robinson, I. S. (2004). Lagrangian and satellite observations of the Brazilian coastal current. *Continental Shelf Research*, *24*(2), 241–262. https://doi.org/10.1016/j.csr.2003.10.001

Dekens, P. S., Lea, D. W., Pak, D. K., & Spero, H. J. (2002). Core top calibration of Mg/Ca in tropical foraminifera: Refining paleotemperature estimation. *Geochemistry, Geophysics, Geosystems*, *3*(4), 1–29. https://doi.org/10.1029/2001GC000200

Deplazes, G., Lückge, A., Peterson, L. C., Timmermann, A., Hamann, Y., Hughen, K. A., et al. (2013). Links between tropical rainfall and North Atlantic climate during the last glacial period. *Nature Geoscience*, *6*(3), 213–217. https://doi.org/10.1038/ngeo1712

Donohoe, A., Marshall, J., Ferreira, D., & Mcgee, D. (2013). The relationship between ITCZ location and cross-equatorial atmospheric heat transport: From the seasonal cycle to the last glacial maximum. *Journal of Climate*, *26*(11), 3597–3618. https://doi.org/10.1175/JCLI-D-12-00467.1

Elderfield, H., Vautravers, M., & Cooper, M. (2002). The relationship between shell size and Mg/Ca, Sr/Ca, $\delta^{18}O$, and $\delta^{13}C$ of species of planktonic foraminifera. *Geochemistry, Geophysics, Geosystems*, *3*(8), 1–13. https://doi.org/10.1029/2001GC000194

Fasullo, J. T., & Trenberth, K. E. (2008). The annual cycle of the energy budget. Part II: Meridional structures and poleward transports. *Journal of Climate*, *21*(10), 2313–2325. https://doi.org/10.1175/2007JCLI1936.1

Fratantoni, D. M., Johns, W. E., Townsend, T. L., & Hurlburt, H. E. (2000). Low-latitude circulation and mass transport pathways in a model of the tropical Atlantic Ocean*. *Journal of Physical Oceanography*, *30*(8), 1944–1966. https://doi.org/10.1175/1520-0485(2000)030<1944:LLCAMT>2.0.CO;2

Friedrich, O., Schiebel, R., Wilson, P. A., Weldeab, S., Beer, C. J., Cooper, M. J., & Fiebig, J. (2012). Influence of test size, water depth, and ecology on Mg/Ca, Sr/Ca, $\delta^{18}O$ and $\delta^{13}C$ in nine modern species of planktic foraminifers. *Earth and Planetary Science Letters*, *319–320*, 133–145. https://doi.org/10.1016/j.epsl.2011.12.002

Gray, W. R., & Evans, D. (2019). Nonthermal Influences on Mg/Ca in Planktonic Foraminifera: A review of culture studies and application to the last glacial maximum. *Paleoceanography and Paleoclimatology*, *34*(3), 306–315. https://doi.org/10.1029/2018PA003517

Greaves, M., Caillon, N., Rebaubier, H., Bartoli, G., Bohaty, S., Cacho, I., et al. (2008). Interlaboratory comparison study of calibration standards for foraminiferal Mg/Ca thermometry. *Geochemistry, Geophysics, Geosystems*, *9*(8), a–n.n/a-n/a. https://doi.org/10.1029/2008GC001974

Gu, F., Chiessi, C. M., Zonneveld, K. A. F., & Behling, H. (2018). Late Quaternary environmental dynamics inferred from marine sediment core GeoB6211-2 off southern Brazil. *Palaeogeography, Palaeoclimatology, Palaeoecology*, *496*, 48–61. https://doi.org/10.1016/j.palaeo.2018.01.015

Heinrich, H. (1988). Origin and Consequences of Cyclic Ice Rafting in the Northeast Atlantic Ocean During the Past 130,000 Years. *Quaternary Research*, *29*(2), 142–152. https://doi.org/10.1016/0033-5894(88)90057-9

Hodell, D. A., Nicholl, J. A., Bontognali, T. R. R., Danino, S., Dorador, J., Dowdeswell, J. A., et al. (2017). Anatomy of Heinrich Layer 1 and its role in the last deglaciation. *Paleoceanography*, *32*(3), 284–303. https://doi.org/10.1002/2016PA003028

Hönisch, B., Allen, K. A., Lea, D. W., Spero, H. J., Eggins, S. M., Arbuszewski, J., et al. (2013). The influence of salinity on Mg/Ca in planktic foraminifers—evidence from cultures, core-top sediments and complementary $\delta^{18}O$. *Geochimica et Cosmochimica Acta*, *121*, 196–213. https://doi.org/10.1016/j.gca.2013.07.028

Laskar, J., Robutel, P., Joutel, F., Gastineau, M., Correia, A. C. M., & Levrard, B. (2004). A long-term numerical solution for the insolation quantities of the Earth. *Astronomy & Astrophysics*, *428*(1), 261–285. https://doi.org/10.1051/0004-6361:20041335

Lippold, J., Pöppelmeier, F., Süfke, F., Gutjahr, M., Goepfert, T. J., Blaser, P., et al. (2019). Constraining the variability of the Atlantic meridional overturning circulation during the Holocene. *Geophysical Research Letters*, *46*(20), 11338–11346. https://doi.org/10.1029/2019GL084988

Locarnini, M., Mishonov, A., Baranova, O., Boyer, T., Zweng, M., Garcia, H., et al. (2018). World ocean atlas 2018 (Vol. 1). Temperature. Retrieved from https://archimer.ifremer.fr/doc/00651/76338/

Locarnini, R. A., Mishonov, A. V., Antonov, J. I., Boyer, T. P., Garcia, H. E., Baranova, O. K., et al. (2013). *World ocean atlas temperature*. (Vol. 1). https://doi.org/10.7289/V55X26VD

Lynch-Stieglitz, J., Schmidt, M. W., & Curry, W. B. (2011). Evidence from the Florida Straits for Younger Dryas ocean circulation changes. *Paleoceanography*, *26*(1). https://doi.org/10.1029/2010PA002032

Maier-Reimer, E., Mikolajewicz, U., & Crowley, T. (1990). Ocean general circulation model sensitivity experiment with an open central American Isthmus. *Paleoceanography*, *5*(3), 349–366. https://doi.org/10.1029/PA005i003p00349

Martin, P. A., & Lea, D. W. (2002). A simple evaluation of cleaning procedures on fossil benthic foraminiferal Mg/Ca. *Geochemistry, Geophysics, Geosystems*, *3*(10), 1–8. https://doi.org/10.1029/2001GC000280

Matano, R. P., Schlax, M. G., & Chelton, D. B. (1993). Seasonal variability in the southwestern Atlantic. *Journal of Geophysical Research*, *98*(C10), 18027–18035. https://doi.org/10.1029/93JC01602

McGee, D., Donohoe, A., Marshall, J., & Ferreira, D. (2014). Changes in ITCZ location and cross-equatorial heat transport at the Last Glacial Maximum, Heinrich Stadial 1, and the mid-Holocene. *Earth and Planetary Science Letters*, *390*, 69–79. https://doi.org/10.1016/j.epsl.2013.12.043

McGee, D., Moreno-Chamarro, E., Green, B., Marshall, J., Galbraith, E., & Bradtmiller, L. (2018). Hemispherically asymmetric trade wind changes as signatures of past ITCZ shifts. *Quaternary Science Reviews*, *180*, 214–228. https://doi.org/10.1016/j.quascirev.2017.11.020

McManus, J. F., Francois, R., Gherardi, J.-M., Keigwin, L. D., & Brown-Leger, S. (2004). Collapse and rapid resumption of Atlantic meridional circulation linked to deglacial climate changes. *Nature*, *428*(6985), 834–837. https://doi.org/10.1038/nature02494

Mohtadi, M., Prange, M., Oppo, D. W., De Pol-Holz, R., Merkel, U., Zhang, X., et al. (2014). North Atlantic forcing of tropical Indian Ocean climate. *Nature*, *509*(7498), 76–80. https://doi.org/10.1038/nature13196

Mulitza, S., Chiessi, C. M., Schefuß, E., Lippold, J., Wichmann, D., Antz, B., et al. (2017). Synchronous and proportional deglacial changes in Atlantic meridional overturning and northeast Brazilian precipitation. *Paleoceanography*, *32*(6), 622–633. https://doi.org/10.1002/2017PA003084

Muschitiello, F., D'Andrea, W. J., Schmittner, A., Heaton, T. J., Balascio, N. L., deRoberts, N., et al. (2019). Deep-water circulation changes lead North Atlantic climate during deglaciation. *Nature Communications*, *10*(1), 1272. https://doi.org/10.1038/s41467-019-09237-3

Pachauri, R. K., Allen, M. R., Barros, V. R., Broome, J., Cramer, W., Christ, R., et al. (2014). *Climate change 2014: Synthesis report. Contribution of working groups I, II and III to the fifth assessment report of the intergovernmental panel on climate change*. Ipcc.

Peterson, R. G., & Stramma, L. (1991). Upper-level circulation in the South Atlantic Ocean. *Progress in Oceanography*, *26*(1), 1–73. https://doi.org/10.1016/0079-6611(91)90006-8

Portilho-Ramos, R. d. C., Ferreira, F., Calado, L., Frontalini, F., & de Toledo, M. B. (2015). Variability of the upwelling system in the southeastern Brazilian margin for the last 110,000 yr. *Global and Planetary Change*, *135*, 179–189. https://doi.org/10.1016/j.gloplacha.2015.11.003

Reißig, S., Nürnberg, D., Bahr, A., Poggemann, D. W., & Hoffmann, J. (2019). Southward displacement of the North Atlantic subtropical gyre circulation system during North Atlantic cold spells. *Paleoceanography and Paleoclimatology*, *34*(5), 866–885. https://doi.org/10.1029/2018PA003376

Reimer, P. J., Bard, E., Bayliss, A., Beck, J. W., Blackwell, P. G., Ramsey, C. B., et al. (2013). IntCal13 and Marine13 radiocarbon age calibration curves 0–50,000 yr cal BP. *Radiocarbon*, *55*(4), 1869–1887. https://doi.org/10.2458/azu_js_rc.55.16947

Rippert, N., Nürnberg, D., Raddatz, J., Maier, E., Hathorne, E., Bijma, J., & Tiedemann, R. (2016). Constraining foraminiferal calcification depths in the western Pacific warm pool. *Marine Micropaleontology*, *128*, 14–27. https://doi.org/10.1016/j.marmicro.2016.08.004

Rühs, S., Getzlaff, K., Durgadoo, J. V., Biastoch, A., & Böning, C. W. (2015). On the suitability of North Brazil Current transport estimates for monitoring basin-scale AMOC changes. *Geophysical Research Letters*, *42*(19), 8072–8080. https://doi.org/10.1002/2015GL065695

Schmidt, M. W., Chang, P., Hertzberg, J. E., Them, T. R., Ji, L., & Otto-Bliesner, B. L. (2012). Impact of abrupt deglacial climate change on tropical Atlantic subsurface temperatures. *Proceedings of the National Academy of Sciences*, *109*(36), 14348–14352. https://doi.org/10.1073/pnas.1207806109

Stainbank, S., Kroon, D., Rüggeberg, A., Raddatz, J., de Leau, E. S., Zhang, M., & Spezzaferri, S. (2019). Controls on planktonic foraminifera apparent calcification depths for the northern equatorial Indian Ocean. *PLOS ONE One*, *14*(9), e0222299. https://doi.org/10.1371/journal.pone.0222299

Stocker, T. F. (1998). Climate Change: The seesaw effect. *Science*, *282*(5386), 61–62. https://doi.org/10.1126/science.282.5386.61

Stocker, T. F., & Johnsen, S. J. (2003). A minimum thermodynamic model for the bipolar seesaw. *Paleoceanography*, *18*(4), a–n. https://doi.org/10.1029/2003PA000920

Stramma, L., & England, M. (1999). On the water masses and mean circulation of the South Atlantic Ocean. *Journal of Geophysical Research*, *104*(C9), 20863–20883. https://doi.org/10.1029/1999JC900139

Stríkis, N. M., Chiessi, C. M., Cruz, F. W., Vuille, M., Cheng, H., de Souza Barreto, E. A., et al. (2015). Timing and structure of Mega-SACZ events during Heinrich Stadial 1. *Geophysical Research Letters*, *42*(13), 5477–5484A. https://doi.org/10.1002/2015GL064048

Talley, L. D., Pickard, G. L., Emery, W. J., & Swift, J. H. (2011). Atlantic Ocean. In L. D. Talley, G. L. Pickard, W. J. Emery, & J. H. Swift (Eds.), Eds., *Descriptive physical oceanography* (6th ed., pp. 245–301). Boston: Academic Press. https://doi.org/10.1016/B978-0-7506-4552-2.10009-5

Thornalley, D. J. R., Barker, S., Broecker, W. S., Elderfield, H., & McCave, I. N. (2011). The Deglacial evolution of North Atlantic deep convection. *Science*, *331*(6014), 202–205. https://doi.org/10.1126/science.1196812

Vellinga, M., & Wu, P. (2008). Relations between Northward Ocean and atmosphere energy transports in a coupled climate model. *Journal of Climate*, *21*(3), 561–575. https://doi.org/10.1175/2007JCLI1754.1

Venancio, I. M., Belem, A. L., Santos, T. P., Lessa, D. O., Albuquerque, A. L. S., Mulitza, S., et al. (2017). Calcification depths of planktonic foraminifera from the southwestern Atlantic derived from oxygen isotope analyses of sediment trap material. *Marine Micropaleontology*, *136*, 37–50. https://doi.org/10.1016/j.marmicro.2017.08.006

Wang, X., Auler, A. S., Edwards, R. L., Cheng, H., Cristalli, P. S., Smart, P. L., et al. (2004). Wet periods in northeastern Brazil over the past 210 kyr linked to distant climate anomalies. *Nature*, *432*(7018), 740–743. https://doi.org/10.1038/nature03067

Weldeab, S., Schneider, R. R., & Kölling, M. (2006). Deglacial sea surface temperature and salinity increase in the western tropical Atlantic in synchrony with high latitude climate instabilities. *Earth and Planetary Science Letters*, *241*(3), 699–706. https://doi.org/10.1016/j.epsl.2005.11.012

Wilson, K. E., Maslin, M. A., & Burns, S. J. (2011). Evidence for a prolonged retroflection of the North Brazil current during glacial stages. *Palaeogeography, Palaeoclimatology, Palaeoecology*, *301*(1), 86–96. https://doi.org/10.1016/j.palaeo.2011.01.003

Yang, H., Wen, Q., Yao, J., & Wang, Y. (2017). Bjerknes compensation in meridional heat transport under freshwater forcing and the role of climate feedback. *Journal of Climate*, *30*(14), 5167–5185. https://doi.org/10.1175/JCLI-D-16-0824.1

Zarriess, M., Johnstone, H., Prange, M., Steph, S., Groeneveld, J., Mulitza, S., & Mackensen, A. (2011). Bipolar seesaw in the northeastern tropical Atlantic during Heinrich stadials. *Geophysical Research Letters*, *38*(4), a–n. https://doi.org/10.1029/2010GL046070

Zhang, D., Msadek, R., McPhaden, M. J., & Delworth, T. (2011). Multidecadal variability of the North Brazil current and its connection to the Atlantic meridional overturning circulation. *Journal of Geophysical Research*, *116*(C4). https://doi.org/10.1029/2010JC006812

Zhang, R., & Delworth, T. L. (2005). Simulated tropical response to a substantial weakening of the Atlantic Thermohaline circulation. *Journal of Climate*, *18*(12), 1853–1860. https://doi.org/10.1175/JCLI3460.1

Zhang, Y., Chiessi, C. M., Mulitza, S., Zabel, M., Trindade, R. I. F., Hollanda, M. H. B. M., et al. (2015). Origin of increased terrigenous supply to the NE South American continental margin during Heinrich Stadial 1 and the Younger Dryas. *Earth and Planetary Science Letters*, *432*, 493–500. https://doi.org/10.1016/j.epsl.2015.09.054

References From The Supporting Information

Arbuszewski, J., deMenocal, P., Kaplan, A., & Farmer, E. C. (2010). On the fidelity of shell-derived $\delta^{18}O$ seawater estimates. *Earth and Planetary Science Letters*, *300*(3), 185–196. https://doi.org/10.1016/j.epsl.2010.10.035

Austermann, J., Mitrovica, J. X., Latychev, K., & Milne, G. A. (2013). Barbados-based estimate of ice volume at Last Glacial Maximum affected by subducted plate. *Nature Geoscience*, *6*(7), 553–557. https://doi.org/10.1038/ngeo1859

Bahr, A., Nürnberg, D., Schönfeld, J., & Garbe-Schönberg, D. (2011). Hydrological variability in Florida Straits during marine isotope stage 5 cold events. *Paleoceanography*, *26*(2). https://doi.org/10.1029/2010PA002015

Barker, S., Greaves, M., & Elderfield, H. (2003). A study of cleaning procedures used for foraminiferal Mg/Ca paleothermometry. *Geochemistry, Geophysics, Geosystems*, *4*(9). https://doi.org/10.1029/2003GC000559

Bemis, B. E., Spero, H. J., Bijma, J., & Lea, D. W. (1998). Reevaluation of the oxygen isotopic composition of planktonic foraminifera: Experimental results and revised paleotemperature equations. *Paleoceanography*, *13*(2), 150–160. https://doi.org/10.1029/98PA00070

Chiessi, C. M., Mulitza, S., Groeneveld, J., Silva, J. B., Campos, M. C., & Gurgel, M. H. C. (2014). Variability of the Brazil Current during the late Holocene. *Palaeogeography, Palaeoclimatology, Palaeoecology*, *415*, 28–36. https://doi.org/10.1016/j.palaeo.2013.12.005

Hönisch, B., Allen, K. A., Lea, D. W., Spero, H. J., Eggins, S. M., Arbuszewski, J., et al. (2013). The influence of salinity on Mg/Ca in planktic foraminifers – Evidence from cultures, core-top sediments and complementary δ18O. *Geochimica et Cosmochimica Acta*, *121*, 196–213. https://doi.org/10.1016/j.gca.2013.07.028

Hou, A., Bahr, A., Raddatz, J., Voigt, S., Greule, M., Albuquerque, A. L., et al. (2020). Insolation and greenhouse gas forcing of the South American monsoon system across three glacial-interglacial cycles. *Geophysical Research Letters*, *47*(14). e2020GL087948. https://doi.org/10.1029/2020GL087948

Hut, G. (1987). *Consultants' group meeting on stable isotope reference samples for geochemical and hydrological investigations*. Retrieved from http://inis.iaea.org/Search/search.aspx?orig_q=RN:18075746

Locarnini, M., Mishonov, A., Baranova, O., Boyer, T., Zweng, M., Garcia, H., et al. (2018). World ocean atlas 2018 (Vol. 1). Temperature. Retrieved from https://archimer.ifremer.fr/doc/00651/76338/

Lynch-Stieglitz, J., Schmidt, M. W., & Curry, W. B. (2011). Evidence from the Florida Straits for Younger Dryas ocean circulation changes. *Paleoceanography*, *26*(1). https://doi.org/10.1029/2010PA002032

Mohtadi, M., Prange, M., Oppo, D. W., De Pol-Holz, R., Merkel, U., Zhang, X., et al. (2014). North Atlantic forcing of tropical Indian Ocean climate. *Nature*, *509*(7498), 76–80. https://doi.org/10.1038/nature13196

Nürnberg, D., Böschen, T., Doering, K., Mollier-Vogel, E., Raddatz, J., & Schneider, R. (2015). Sea surface and subsurface circulation dynamics off equatorial Peru during the last 17 kyr. *Paleoceanography*, *30*(7), 984–999. https://doi.org/10.1002/2014PA002706

Ostlund, H. G., Craig, H., Broecker, W. S., & Spenser, D. (1987). GEOSECS Atlantic, Pacific, and Indiean Ocean expeditions Shorebased data and graphics (Vol. 7, pp. 1–200). Washington, D. C.: Natl. Sci. Found.

Pierre, C., Vergnaud-Grazzini, C., & Faugeres, J. C. (1991). Oxygen and carbon stable isotope tracers of the water masses in the Central Brazil Basin. Deep Sea Research Part A. *Oceanographic Research Papers*, *38*(5), 597–606. https://doi.org/10.1016/0198-0149(91)90065-N

Raymo, M. E., Kozdon, R., Evans, D., Lisiecki, L., & Ford, H. L. (2018). The accuracy of mid-Pliocene δ18O-based ice volume and sea level reconstructions. *Earth-Science Reviews*, *177*, 291–302. https://doi.org/10.1016/j.earscirev.2017.11.022

Schmidt, G. A. (1999). *Global seawater oxygen-18 database*. Retrieved from https://ci.nii.ac.jp/naid/10019631520/. http://Data.Giss.Nasa.Gov/O18data/